Theoretical investigation of electron-impact double ionization of B-like C^+ to Ne^{5+} ions

Yulong Ma,[1,*] Ling Liu,[2] Yong Wu,[2,3] Luyou Xie,[1] Yizhi Qu,[4] and Jianguo Wang[2]
[1]*College of Physics and Electronic Engineering, Northwest Normal University, Lanzhou 730070, China*
[2]*Key Laboratory of Computational Physics, Institute of Applied Physics and Computational Mathematics, Beijing 100088, China*
[3]*HEDPS, Center for Applied Physics and Technology, Peking University, Beijing 100084, China*
[4]*School of Optoelectronics, University of Chinese Academy of Sciences, Beijing 100049, China*

(Received 25 July 2022; accepted 2 March 2023; published 14 March 2023)

Electron-impact double ionization (DI) including direct and indirect processes of B-like C^+ to Ne^{5+} ions is investigated using a two-step approach. The direct process is treated as a primary single ionization (SI) and subsequent knockout mechanism. The indirect process is considered as a primary SI of an inner-shell 1*s* electron followed by a single autoionization. Based on the two-step approach, the DI cross sections are calculated using flexible atomic code with distorted-wave approximation. The potential of the intermediate ion is approximately equivalent to the mean potential constructed by three ions involved for calculating the cross section of the direct process, while using the potential of the ionizing ion in each step of the present two-step approach overestimates results. The present cross sections agree with available theoretical and experimental data.

DOI: 10.1103/PhysRevA.107.032813

I. INTRODUCTION

Electron-impact double ionization (DI) processes are of critical importance for fundamental problems [1] and in applications related to investigations of laboratory and astrophysical plasmas [2,3] as well as tumor therapy physics [4]. Generally, two competing processes of direct double ionization (DDI) and indirect double ionization (IDI) are responsible for the DI process. The DDI and IDI result in the final ion via an emission of two ejected electrons simultaneously and sequentially in a stepwise way, respectively [5].

A large amount of experimental data on electron-impact DI cross sections of atoms and ions is available for helium through zinc elements, as reviewed recently by Hahn *et al.* [6]. The DI processes of the heavier ions also have been investigated widely [7–10]. Whereas accurate cross sections of single ionization (SI) can be calculated by several numerical methods, the DI process still need to be interpreted. However, theoretical difficulties arise very rapidly due to the complex nature of the four-body Coulomb problem in a DI process [1].

The nonperturbative time-dependent close coupling (TDCC) method [11] has been employed to calculate DDI cross sections for two-electron helium [12]. However, computations of the TDCC challenge the computational capability for complex atomic systems. In addition, the DDI has been considered as two-step (TS), i.e., TS1 and TS2 mechanisms. In a classical picture [13], the incident electron collides with the target ion, emitting an ejected electron, and then this ejected electron collides with the remaining ion to remove another bound electron for the TS1. The incident electron collides with the target ion and removes two bound electrons sequentially in the TS2. Recently, this classical picture was extended to treat the DDI as a sequence of two- and three-step processes [14–18]. Later, the TS approach based on knockout (KO) mechanism has been proposed to deal with the DDI process, which has been able to accurately predict DDI cross sections [19,20]. Furthermore, we extended the KO mechanism to deal with the direct process of the electron-impact triple ionization [20].

Many experimental cross sections have been obtained for the DI process of B-like ions such as C^+ [21–23], N^{2+} [22], O^{3+} [22], and Ne^{5+} [24]. It has been found that DI cross sections are contributed dominantly by DDI processes at the incident energy below the ionization threshold of inner-shell 1*s* electron [24,25]. Besides, the IDI also contributes to the process for light B-like ions, which considers only the simple channel with a primary SI of an inner-shell 1*s* electron followed by a single autoionization (SA) [23–25]. Hence, to some extent, IDI cross sections can be calculated with satisfactory accuracy. Besides, the experimental measurements found the contribution of metastable states to be negligible for the SI of C^+ [26,27]. Moreover, the ion population due to metastable states was found to be negligible for the DI of Ne^{5+} [24]. Therefore, the boron isoelectronic sequence could be a good candidate for testing theories on DI processes with the basis of the available experimental data.

In the present work, the DI with inclusion of the DDI and IDI processes are investigated theoretically by utilizing the TS approach for the B-like C^+, N^{2+}, O^{3+}, F^{4+}, and Ne^{5+} ions. The DI cross sections are calculated by using flexible atomic code (FAC) [28] based on the fully relativistic distorted-wave (DW) approximation. Moreover, influences of adopting different central potential constructed in FAC are discussed on calculations of the DDI cross section. The present results are compared with available theoretical and experimental data.

The remainder of the paper is structured as follows. Section II describes the theoretical approach for calculating the

*mayulong@nwnu.edu.cn

DDI and IDI cross sections. The present cross sections are compared with available theoretical and experimental values, and corresponding discussions are given in Sec. III. Conclusions are provided in Sec. IV. Calculated results of F^{4+} ion are shown in the Appendix due to absence of available experimental data for comparison.

II. THEORETICAL METHOD

The DDI channel results in a final ion of charge state $(q+2)+$ for an initial target ion of charge state $q+$, which can be described as

$$e^- + A^{q+} \xrightarrow{\text{DDI}} A^{(q+2)+} + 3e^-. \quad (1)$$

In the DDI, two electrons in the target ion are ionized simultaneously by the electron impact.

Two electrons in the target ion could be ionized in a stepwise manner through the creation and decay of intermediate autoionizing states in the IDI process. It can be described as a primary SI of an electron (inner-shell electron in general) producing intermediate autoionizing states $A^{*(q+1)+}$, which emits another electron via a SA

$$e^- + A^{q+} \xrightarrow{\text{SI}} A^{*(q+1)+} + 2e^- \xrightarrow{\text{SA}} A^{(q+2)+} + 3e^-. \quad (2)$$

The IDI process also occurs when the initial state of the target A^{q+} ion is excited to the autoionizing state A^{*q+}, which could decay through double autoionization (DA) to the $A^{(q+2)+}$ ion. This IDI is known as the excitation DA process. Besides, higher order multiple autoionization processes could involve due to dielectronic capture (DC). The DC will reduce the charge of the target ion and form to a resonant state $A^{**(q-1)+}$. Such resonant state decays by the triple autoionization (TA) to form an $A^{(q+2)+}$ ion. This is referred to as resonant excitation TA. However, neither of these processes with DA and TA are expected to contribute significantly to the total DI cross section for B-like ions. This is supported by Ref. [19] for B-like C^+. Moreover, characteristics of the DI cross section due to the high-order DA and TA are not found in experimental findings [21–24].

We consider the DDI and IDI processes as independent. Thus, the DI cross section of $\sigma^{\text{DI}}(\varepsilon_0)$ from initial state i to final state f is obtained by a sum of the DDI cross section of $\sigma^{\text{DDI}}(\varepsilon_0)$ and IDI cross section of $\sigma^{\text{IDI}}(\varepsilon_0)$ at the incident energy of ε_0. Then the total DI cross section is given by

$$\sigma_{if}^{\text{DI}}(\varepsilon_0) = \sigma_{if}^{\text{DDI}}(\varepsilon_0) + \sigma_{if}^{\text{IDI}}(\varepsilon_0). \quad (3)$$

In our previous study, we proposed a TS approach based on the KO mechanism to deal with the DDI process [20]. Such mechanism also has been applied successfully to the DI by absorption of one [29,30] or two [31] photons, the multiple-Auger decay [32–37], the double-K-vacancy production in ion-atom collisions [38,39], and the DI of a molecule by interatomic Coulombic decay [40].

In addition to the KO mechanism, the shakeoff (SO) mechanism could contribute to the DDI process. In the SO mechanism, the primary ejected electron is emitted rapidly due to the electron impact with ion. Thus the sudden change of the potential is felt by the remaining electrons of ion, which results in subsequent relaxation leading to the ejection of the second electron. However, the SO mechanism is weak for the low and intermediate energies [41]. At the high energy, although the SO mechanism might be important to the DDI, it still has a negligible impact on the total DI cross section because contributions from the IDI become dominant and those of the DDI are so weak to the total DI in the present cases of B-like ions at the high enough energy. This has been illustrated in Ref. [19] and our previous work [20]. Therefore, contributions of the SO mechanism are neglected in the present work.

The KO mechanism describes the correlated dynamics of electrons: A bound electron in an ion is knocked out via an $(e, 2e)$-like process [29]. The $(e, 2e)$ is used as a proxy term for the electron-impact ionization. Thus, we decompose the DDI into the primary SI and the subsequent KO process

$$e^- + A^{q+} \xrightarrow{\text{SI}} A^{(q+1)+} + 2e^- \xrightarrow{\text{KO}} A^{(q+2)+} + 3e^-. \quad (4)$$

Consequently, the DDI cross section from initial state i to final state f can be obtained by following expression:

$$\sigma_{if}^{\text{DDI}}(\varepsilon_0) = \sum_m \sigma_{im}^{\text{SI}}(\varepsilon_0) \int_{I_{mf}}^{\varepsilon_0 - I_{im}} \rho_{im}(\varepsilon_0, \varepsilon) \Omega_{mf}^{\text{KO}}(\varepsilon) d\varepsilon. \quad (5)$$

Here, $\sigma_{im}^{\text{SI}}(\varepsilon_0)$ is the cross section of the primary SI from initial state i to intermediate state m. In the primary SI, two intermediate electrons are emitted simultaneously and share the excess energy of $\varepsilon_0 - I_{im}$, where I_{im} is the primary SI threshold. Note that any one of the intermediate electrons will participate in the subsequent KO process, and we assume that one of the intermediate electrons takes the energy ranging from zero to $\varepsilon_0 - I_{im}$. $\Omega_{mf}^{\text{KO}}(\varepsilon)$ is the KO collision strength by intermediate electrons with energy ε. Thus, the energy distribution is needed to be introduced in the present TS treatment of the DDI, as proposed in our previous work [20]. Such energy distribution can be determined by using the differential cross sections of the primary SI, which could be calculated by using the analytic binary-encounter formula [42]. The energy distribution should be normalized to unity on the energy scale, $\int_0^{\varepsilon_0 - I_{im}} \rho_{im}(\varepsilon_0, \varepsilon) d\varepsilon = 1$. It should be noted that the intermediate electron with the energy $0 \leqslant \varepsilon < I_{mf}$ is energetically forbidden to ionize a bound electron of the intermediate ion, where I_{mf} is the ionization threshold of the intermediate ionic state. Therefore, the contributions of all intermediate electrons can be included by integrating over the energy from I_{mf} to $\varepsilon_0 - I_{im}$ in Eq. (5). Currently, the energy distribution was implemented to study multiple ionization by electron impact using a sequence of few-step processes [18]. Besides, we have also used energy distributions of intermediate electrons to investigate direct multiple Auger processes [33,34,36].

For light B-like ions, the IDI process can be generally described as the primary SI of an inner-shell $1s$ electron and a subsequent SA. The corresponding cross section can be obtained from

$$\sigma_{if}^{\text{IDI}}(\varepsilon_0) = \sum_m \sigma_{im}^{\text{SI}}(\varepsilon_0) B_{mf}^{\text{SA}}, \quad (6)$$

where $\sigma_{im}^{\text{SI}}(\varepsilon_0)$ is the SI cross section from initial state i to the intermediate state m with $1s$ hole, which can then undergo SA

with a branching ratio

$$B_{mf}^{\mathrm{SA}} = \frac{A_{mf}^{a}}{\sum_k A_{mk}^{a} + \sum_s A_{ms}^{r}}, \tag{7}$$

where $\sum_k A_{mk}^{a}$ and $\sum_s A_{ms}^{r}$ are the total rates of intermediate state m via the SA process and the radiative stabilization, respectively. A_{mf}^{a} is the SA rate from intermediate state m to final state f. In the present cases of B-like ions with $6 \leqslant Z \leqslant 10$, we neglect all radiative decay processes which are typically suppressed by several orders of magnitude [43].

The FAC [28] is employed to obtain the SI cross section and the collision strength of the KO mechanism, which implements the DW approximation for the continuum electron.

III. RESULTS AND DISCUSSION

Electron correlations lead dominantly to the electron-impact DI, thus which could play an essential role in accurate calculations of the DI cross section [20]. Based on the present TS approach, the calculations of DDI cross section concern three different successive ionization stages, i.e., initial B-like, intermediate Be-like, and final Li-like ions. Therefore, one should consider the balance of electron correlation for the ions with different ionization stages when using the standard configuration interaction procedure. In configuration interaction approximation implemented in the FAC [28], the configurations produced by single and double excitations from the respective ground configurations of B-, Be-, and Li-like ions to the orbitals of $2l$, $3l$, and $4l$ are considered for including electron correlations on the equal footing. Therefore, the interactions among the following configurations are included: $[2s, 2p]^m$, $[2s, 2p]^{m-1}3l$, $[2s, 2p]^{m-1}4l$, $[2s, 2p]^{m-2}3l^2$, $[2s, 2p]^{m-2}3l4l$, and $[2s, 2p]^{m-2}4l^2$, where $[2s, 2p]^x$ indicates that x electrons are distributed between the $2s$ and $2p$ orbitals. Here, $m = 5$ for B-like ion, $m = 4$ for Be-like ion, and $m = 3$ for Li-like ion.

In FAC, the continuum orbitals are obtained by solving the Dirac equations with the same central potential as that for bound orbitals [28]. It has been demonstrated that using different central potential affects the calculated cross sections for the SI and DI processes [44–46]. Therefore, to explore the influences of central potential on the calculations of the DDI cross section, we generate the central potential in FAC by using following three models.

In model I, the central potential is constructed by the ground configuration $1s^2 2s^2 2p$ of the initial B-like ion and $1s^2 2s^2$ of the intermediate Be-like ion for the primary SI and subsequent KO processes, respectively. It can be also described as that the potential of the ionizing ion is adopted in the first step and one of the ionizing ion is adopted in the second step for the present TS approach. In model II, the central potential is constructed by using the ground configuration $1s^2 2s^2$ of the intermediate Be-like for both of the primary SI and subsequent KO (i.e., the potential of the ionized ion in the first step and that of the ionizing ion in the second step). In model III, the central potential is constructed by the mean configuration consisting of $1s^2 2s^2 2p$, $1s^2 2s^2$, and $1s^2 2s$ for both of the primary SI and subsequent KO. This means that the potential constructed by three ions involved are used in each step.

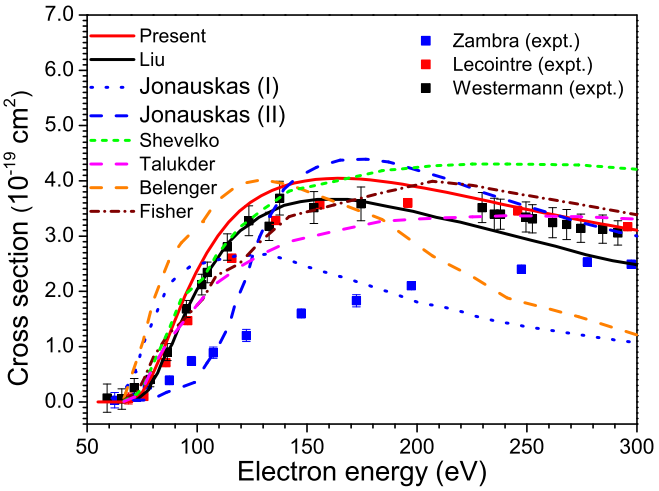

FIG. 1. Cross sections of the electron-impact direct double ionization for C^+ ion. The present results are compared with theoretical results by Liu *et al.* [19], Jonauskas *et al.* [14], Shevelko *et al.* [25], Talukder *et al.* [47], Bélenger *et al.* [48], and Fisher *et al.* [49] as well as experimental values by Zambra *et al.* [21], Westermann *et al.* [22], and Lecointre *et al.* [23]. The present results are obtained in model II (see the text for explanations on model II). Jonauskas (I) and Jonauskas (II) denote theoretical results by Jonauskas *et al.* [14] for the cases of low and intermediate-high incident electron energies, respectively.

A. Cross sections of electron-impact direct double ionization

Now, we focus exclusively on the DDI process. Hence, we restrict the incident energies that lead insufficiently to IDI processes.

In Fig. 1, our DDI cross sections in model II are compared with available theoretical [14,19,25,47–49] and experimental [21–23] results for C^+ ion. As seen in Fig. 1, the experimental results obtained by Zambra *et al.* [21] (in 1994) significantly differ from the other two latest measurements by Westermann *et al.* [22] (in 1999) and Lecointre *et al.* [23] (in 2013). These two results by Westermann *et al.* [22] and by Lecointre *et al.* [23] agree with each other, while the measurements by Zambra *et al.* [21] show not only lower cross sections but also significantly different cross-section tendency. Note that such differences are also found for other cases of N^+ and O^+ ions as shown in the paper [23]. Since the origin of these discrepancies are not clear, the present results are compared with two latest measurements by Westermann *et al.* [22] and Lecointre *et al.* [23]. It is found that the present results agree with the latest measurements [22,23].

The results of Liu *et al.* [19] are calculated based on the KO and SO mechanisms. We note that contributions of the SO to the DDI cross sections are negligible [19], which is also true for O^+ ion in our previous work [20]. It is found that the values of Liu *et al.* [19] are lower by about 10% than our results. However, both of these two theoretical results are in overall agreement with the latest experimental results [22,23]. Compared with the results of Jonauskas *et al.* [14], our results and ones of Liu *et al.* [19] based on KO mechanism provide a considerable improvement in agreement with experimental data. As has been illustrated in our work [20], such

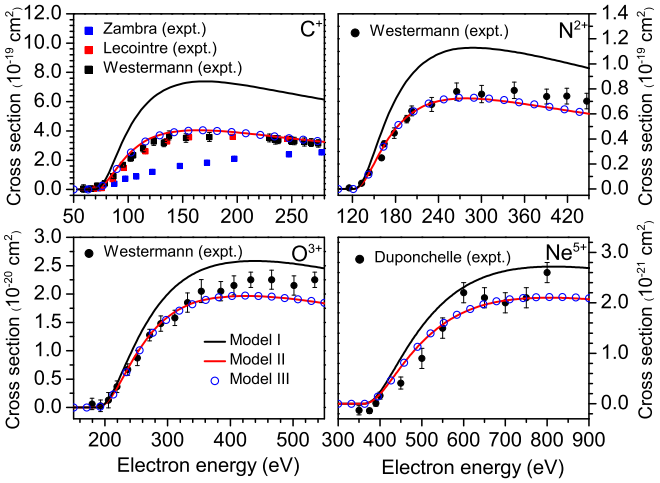

FIG. 2. Cross sections of the electron-impact direct double ionization for C^+, N^{2+}, O^{3+}, and Ne^{5+} ions. The present results are compared with experimental measurements by Zambra *et al.* [21], Westermann *et al.* [22], Lecointre *et al.* [23], and Duponchelle *et al.* [24]. The present results are calculated in models I, II, and III (see the text for explanations on models I, II, and III). The results in model II are taken from our previous work [20] for O^{3+} ion.

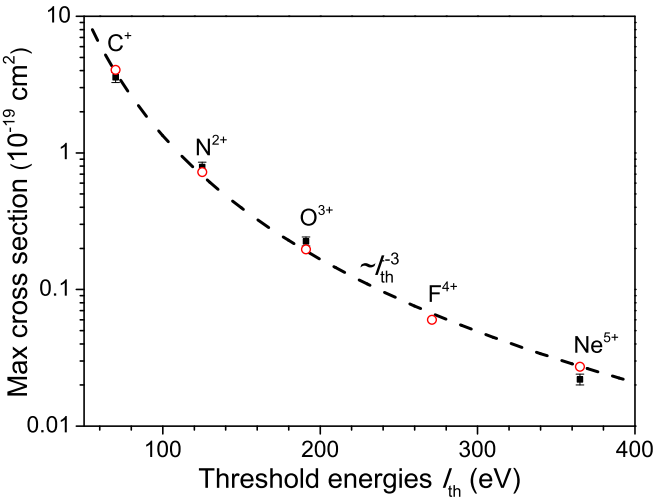

FIG. 3. The present and experimental [22,24] maxima of cross sections vs the double ionization threshold I_{th} for the electron-impact direct double ionization of B-like C^+, N^{2+}, O^{3+}, F^{4+}, and Ne^{5+} ions. The dashed line represents the dependence of $\sim I_{th}^{-3}$. The present results are obtained in model II (see the text for explanations on model II).

improvement are mainly attributed to the energy distributions of intermediate electrons in the TS approach. Due to absence of the proper energy distribution, Jonauskas *et al.* [14] had to calculate two different results to compare with experimental results. Specifically, in the case of low incident energies, all the excess energy after the primary SI is taken by the intermediate electron, which is denoted as Jonauskas (I) in Fig. 1. For the intermediate-high incident energies, the excess energy is shared between the intermediate electrons, which is denoted as Jonauskas (II).

In addition, theoretical results of Shevelko *et al.* [25], Talukder *et al.* [47], Belenger *et al.* [48], and Fisher *et al.* [49] were obtained by semiempirical methods in Fig. 1. It is found that discrepancies between these theoretical results [25,47–49] obtained by semiempirical methods and experimental results [22,23] are observed.

Figure 2 shows the present DDI cross sections for B-like C^+, N^{2+}, O^{3+}, and Ne^{5+} ions, which are compared with the available experimental data [21–24]. Here the present DDI cross sections are calculated by using different central potentials in models I, II, and III. Additionally, the cross sections of DDI as a function of the incident energy are obtained for F^{4+} ion, which are shown in the Appendix. To the best of our knowledge, no experimental results of F^{4+} ion are available for comparison.

It is found in Fig. 2 that the cross sections in model II and those in model III are almost identical, both of which are in reasonably good agreement with experimental data by Westermann *et al.* [22] and Lecointre *et al.* [23]. On the other hand, the DDI cross sections in model I are about 85% greater than calculations in models II and III for C^+ ion. In other cases of N^{2+}, O^{3+}, and Ne^{5+} ions, differences of the results between models II and III are hardly observed, both of which are smaller than the results in model I. Similar to the case of C^+, the results from models II and III provide an overall good agreement with the measurements, while the results in both of models II and III are slightly smaller than the measurements at the higher energy for N^{2+} and O^{3+} ions. It is worth pointing out that the higher energy means the more intermediate states are involved in Eq. (5), which are considered in a limited manner in our calculations due to rapidly increasing computational complexity. Therefore, this might be one of reasons for such differences at higher energies for N^{2+} and O^{3+} ions. These indicate that either the potential of the intermediate ion or the mean potential constructed by three ions involved is proper for the present TS approach based on KO mechanism, and they are approximatively equivalent.

It is found in Fig. 2 that the differences of the results between models I and II decrease with increasing atomic number Z. For example, such difference is about 85% for C^+ ion, while it is reduced to be about 35% for Ne^{5+} ion. It is expected that the differences of asymptotic potentials due to one more or less bound electron become small with increasing Z, as such asymptotic potentials felt by the continuum electron are determined to be $V(r \to \infty) \sim \frac{(Z-N)}{r}$ screened by N bound electrons.

Figure 3 displays the maxima of the DDI cross section as a function of the DI threshold for C^+, N^{2+}, O^{3+}, F^{4+}, and Ne^{5+} ions, along with available experimental maxima [22,24]. In the present cases of B-like ions, the maxima of DDI cross sections appear at incident energy of about two times of the DI threshold. For an isoelectronic sequence, the maxima of the DDI cross sections show a dependence on the DI threshold I_{th}, which are proportional to I_{th}^{-3} [25]. Such dependence $\sim I_{th}^{-3}$ is found for both of our results and experimental data. This also implies that our results of the DDI for F^{4+} are reliable. As shown in Fig. 3, the DDI cross sections decrease rapidly with increasing atomic number. For example, the maxima of the DDI cross section of Ne^{5+} ion is smaller than that of C^+ ion by about two orders of magnitude.

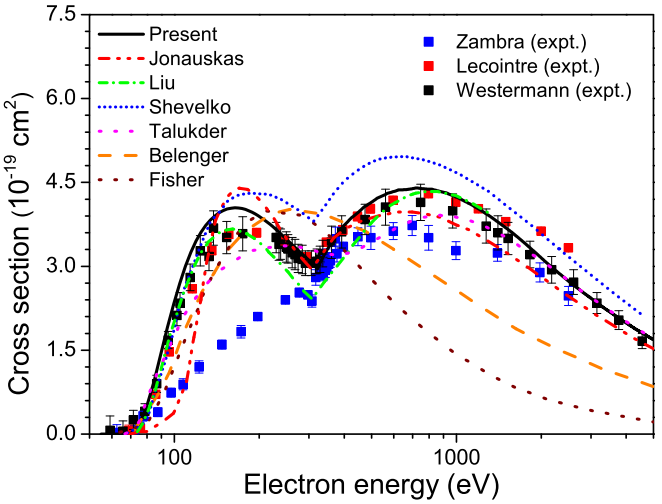

FIG. 4. Total cross sections of the electron-impact double ionization for C^+ ion. The present results are compared with experimental measurements by Zambra *et al.* [21], Westermann *et al.* [22], and Lecointre *et al.* [23] as well as theoretical results by Liu *et al.* [19], Jonauskas *et al.* [14], Shevelko *et al.* [25], Talukder *et al.* [47], Bélenger *et al.* [48], and Fisher *et al.* [49]. The present direct-ionization cross sections are obtained in model II (see the text for explanations on model II).

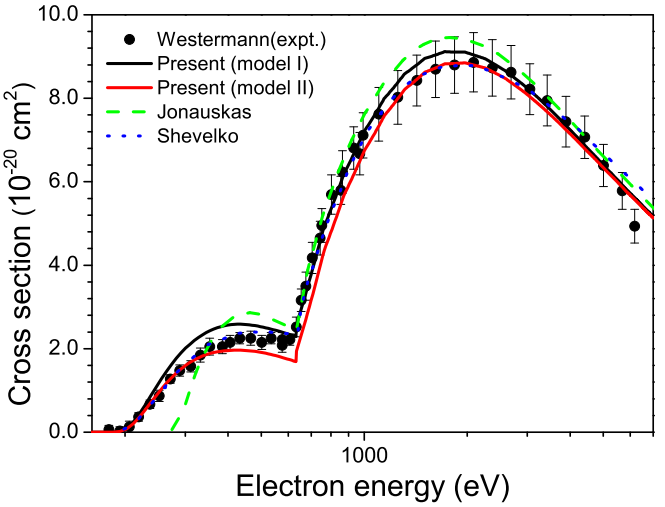

FIG. 5. Total cross sections of the electron-impact double ionization for O^{3+} ion. The present results are compared with experimental results by Westermann *et al.* [22] and theoretical results by Jonauskas *et al.* [14] and Shevelko *et al.* [25]. The cross sections are calculated in models I and II for the direct process (see the text for explanations on models I and II).

B. Total cross sections of electron-impact double ionization

In this subsection, we extend the incident energy up to values that lead to the IDI process. Therefore, the total DI cross sections contribute from the DDI and IDI processes.

Figure 4 shows the present total DI cross sections of C^+ ion, which are compared with available experimental [21–23] and theoretical [14,19,25,47] results. Note that the present cross sections of the DDI are calculated in model II. For incident energies from the ionization threshold to about 315 eV, the DI originates solely from the DDI, which are discussed above in Sec. II. With increasing incident energy, channels of the 1*s* ionization are opened and the IDI processes begin to play a role. The results of Belenger *et al.* [48] and Fisher *et al.* [49] are obviously lower than experimental data, while Shevelko *et al.* [25] predicted a larger cross section. However, other theoretical results including our results agree with available experimental measurements [21–23].

In Fig. 5, the present total cross sections are compared with available experimental [22] and theoretical [14,25] results for O^{3+} ion. Only the DDI contributes to DI at energies from the ionization threshold to about 630 eV. For such energy range, these are discussed above in Sec. II. With increasing incident energy, the present results in model II are slightly lower than the experimental data, particularly at around the threshold of the IDI process. However, the improvement in agreement with measurements can be obtained for the DDI cross section calculated in model I. It indicates that the present calculations can agree with available measurements by using different central potentials. Thus, we look forward to forthcoming experiments that identify the individual contributions from the DDI and IDI processes to test theory. In addition, our results agree also with available theoretical results [14,25].

In Fig. 6, the present total DI cross sections of C^+, N^{2+}, O^{3+}, and Ne^{5+} are compared with available experimental results [21–24]. Here the DDI cross sections are obtained in model II. The total DI cross sections of F^{4+} ion are also calculated and shown in the Appendix. It is found that the overall agreements between the present calculations and experimental data are obtained at the present energy range. Note that the present results overestimate the experimental values [24] for Ne^{5+} ion at the energies greater than about 1500 eV.

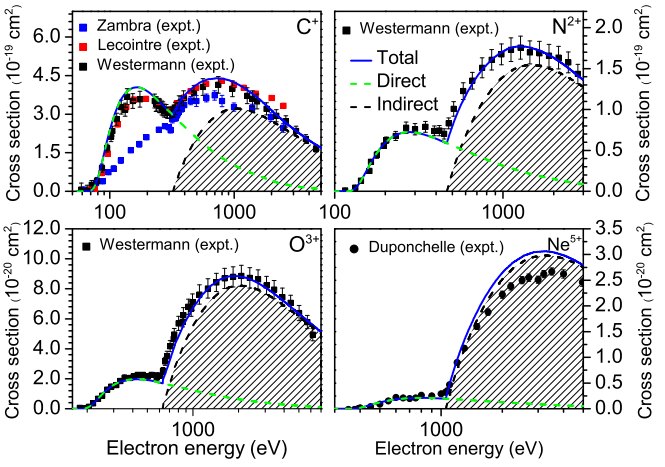

FIG. 6. Total cross sections of the electron-impact double ionization for C^+, N^{2+}, O^{3+}, and Ne^{5+} ions. The present results are compared with experimental measurements by Zambra *et al.* [21], Westermann *et al.* [22], Lecointre *et al.* [23], and Duponchelle *et al.* [24]. Total denotes the total cross sections including the direct ionization cross sections (denoted as Direct) and indirect cross sections (denoted as Indirect). The cross sections of the direct process are calculated in model II (see the text for explanations on model II). The results are taken from our previous work [20] for O^{3+} ion.

As found in Fig. 6, total DI cross sections show a two-peak structure. The first and second peaks result from the DDI and IDI processes, respectively. The maxima of the IDI cross sections (with the shaded areas in Fig. 6) are decreased by about one orders of magnitude from C^+ to Ne^{5+}, while that of DDI cross section are decreased by about two orders of magnitude (as discussed above and shown in Fig. 3). For example, these two maxima are comparable for C^+ ion, while the maxima of DDI are far smaller than those of IDI by about an order of magnitude for Ne^{5+} ion. Hence, DDI cross sections decrease more rapidly than those of the IDI process with increasing atomic number, which is also observed in other isoelectronic sequences [6]. This predicts that the IDI is dominant to the total DI cross section while the DDI is very weak for heavier highly charged B-like ions with $Z > 10$. This also implies that the contributions of DDI processes become small for highly charged ions, as illustrated by our recent work for Fe^{12+} ion [50].

IV. CONCLUSION

The theoretical investigations of the DI process of B-like C^+, N^{2+}, O^{3+}, F^{4+}, and Ne^{5+} ions are presented. Two different and competing processes of the DDI and IDI are included for the DI. The IDI is considered as a TS process that involves a primary SI of an inner-shell 1*s* electron followed by a SA. The TS approach based on KO mechanism is utilized to describe the DDI process that is decomposed into the primary SI and the subsequent KO process. Based on the TS approach, DI cross sections are calculated by using FAC with DW approximation. For calculating the DDI cross sections, the central potential of intermediate Be-like ion (i.e., model II) are basically equivalent to the mean one constructed by three ions involved (i.e., model III) in the present TS approach. Moreover, DDI cross sections obtained by both of models II and III agree well with available experimental data, while using the central potential of the ionizing ion in the each step (i.e., model I) significantly overestimates the DDI cross section. With increasing atomic number, the influences of different central potentials become small on the calculations of the DDI cross section. The present total cross sections including the contributions from the DDI and IDI processes are compared with the available experimental and theoretical data, and the overall agreements are obtained.

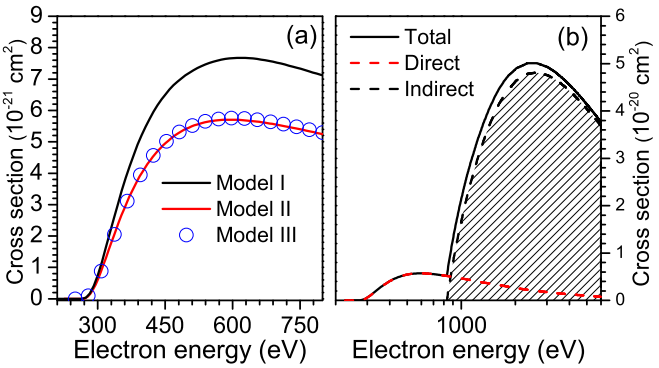

FIG. 7. Cross sections of electron-impact double ionization for F^{4+} ion. (a) The present cross sections are given in models I, II, and III for the direct process (see the text for explanations on models I, II, and III); (b) the present total cross sections of electron-impact double ionization including the the direct and indirect processes. The direct-process results are calculated in model II for total cross sections.

ACKNOWLEDGMENTS

This work was supported by the National Key R&D Program of China (Grant No. 2022YFA1602500), the National Natural Science Foundation of China (Grants No. 12104373, No. 11934004 and No. 12064041), and Heavy Ion Research Facility in Lanzhou (HIRFL) (Grant No. HIR2021PY006).

APPENDIX: CROSS SECTIONS OF THE ELECTRON-IMPACT DOUBLE IONIZATION FOR B-LIKE F^{4+} ION

Figure 7 displays the DDI cross sections in models I, II, and III as well as the total DI cross sections of F^{4+} ion. Here the DDI cross sections in model II are used to obtain the total DI cross sections. From Fig. 7(a), no significant differences of the results between models II and II are found, both of which are smaller by about 40% than the results in model I. For the total DI cross section in Fig. 7(b), the contributions from the IDI process are dominant and are greater than those of the DDI process by about an order of magnitude.

[1] J. Berakdar, A. Lahmam-Bennani, and C. D. Cappello, Phys. Rep. **374**, 91 (2003).
[2] M. Hahn and D. W. Savin, Astrophys. J. **800**, 68 (2015).
[3] M. Hahn and D. W. Savin, Astrophys. J. **809**, 178 (2015).
[4] Y. Zheng, D. J. Hunting, P. Ayotte, and L. Sanche, Phys. Rev. Lett. **100**, 198101 (2008).
[5] A. Müller, Adv. At. Mol. Phys. **55**, 293 (2008).
[6] M. Hahn, A. Müller, and D. W. Savin, Astrophys. J. **850**, 122 (2017).
[7] K. Aichele, W. Arnold, H. Bräuning, D. Hathiramani, F. Scheuermann, R. Trassl, and E. Salzborn, Nucl. Instrum. Methods Phys. Res., Sect. B **205**, 437 (2003).
[8] M. Stenke, K. Aichele, D. Hathiramani, G. Hofmann, M. Steidl, R. Volpel, V. P. Shevelko, H. Tawara, and E. Salzborn, J. Phys. B: At. Mol. Opt. Phys. **28**, 4853 (1995).
[9] M. Stenke, U. Hartenfeller, K. Aichele, D. Hathiramani, M. Steidl, and E. Salzborn, J. Phys. B: At. Mol. Opt. Phys. **32**, 3641 (1999).
[10] B. Fabian, A. Müller, H. Bräuning, J. Jacobi, F. A. Scheuermann, and E. Salzborn, J. Phys. B: At. Mol. Opt. Phys. **38**, 2833 (2005).
[11] M. S. Pindzola, F. Robicheaux, S. D. Loch, J. C. Berengut, T. Topcu, J. Colgan, M. Foster, D. C. Griffin, C. P. Ballance, D. R. Schultz, T. Minami, N. R. Badnell, M. C. Witthoeft, D. R.

Plante, D. M. Mitnik, J. A. Ludlow, and U. Kleiman, J. Phys. B: At. Mol. Opt. Phys. **40**, R39 (2007).
[12] M. S. Pindzola, F. J. Robicheaux, J. P. Colgan, M. C. Witthoeft, and J. A. Ludlow, Phys. Rev. A **70**, 032705 (2004).
[13] M. Gryziński, Phys. Rev. **138**, A336 (1965).
[14] V. Jonauskas, A. Prancikevičius, Š. Masys, and A. Kynienė, Phys. Rev. A **89**, 052714 (2014).
[15] J. Koncevičiūtė and V. Jonauskas, Phys. Rev. A **93**, 022711 (2016).
[16] J. Koncevičiūtė, S. Kučas, Š. Masys, A. Kynienė, and V. Jonauskas, Phys. Rev. A **97**, 012705 (2018).
[17] J. Koncevičiūtė, S. Kučas, A. Kynienė, Š. Masys, and V. Jonauskas, J. Phys. B: At. Mol. Opt. Phys. **52**, 025203 (2019).
[18] J. Koncevičiūtė and V. Jonauskas, Phys. Rev. A **104**, 042804 (2021).
[19] P. Liu, J. Zeng, and J. Yuan, J. Phys. B: At. Mol. Opt. Phys. **51**, 075202 (2018).
[20] Y. Ma, L. Liu, Y. Wu, Y. Qu, and J. Wang, Phys. Rev. A **101**, 052703 (2020).
[21] M. Zambra, D. Belic, P. Defrance, and D. J. Yu, J. Phys. B: At. Mol. Opt. Phys. **27**, 2383 (1994).
[22] M. Westermann, F. Scheuermann, K. Aichele, U. Hartenfeller, D. Hathiramani, M. Steidl, and E. Salzborn, Phys. Scr. **T80B**, 285 (1999).
[23] J. Lecointre, K. A. Kouzakov, D. S. Belic, P. Defrance, Y. V. Popov, and V. P. Shevelko, J. Phys. B: At. Mol. Opt. Phys. **46**, 205201 (2013).
[24] M. Duponchelle, M. Khouilid, E. M. Oualim, H. Zhang, and P. Defrance, J. Phys. B: At. Mol. Opt. Phys. **30**, 729 (1997).
[25] V. P. Shevelko, H. Tawara, F. Scheuermann, B. Fabian, A. Müller, and E. Salzborn, J. Phys. B: At. Mol. Opt. Phys. **38**, 525 (2005).
[26] I. Yamada, A. Danjo, T. Hirayama, A. Matsumoto, S. Ohtani, H. Suzuki, T. Takayanagi, H. Tawara, K. Wakiya, and M. Yoshino, J. Phys. Soc. Jpn. **58**, 1585 (1989).
[27] J. A. Ludlow, S. D. Loch, M. S. Pindzola, C. P. Ballance, D. C. Griffin, M. E. Bannister, and M. Fogle, Phys. Rev. A **78**, 052708 (2008).
[28] M. F. Gu, Can. J. Phys. **86**, 675 (2008).
[29] T. Schneider, P. L. Chocian, and J. M. Rost, Phys. Rev. Lett. **89**, 073002 (2002).
[30] T. Schneider and J.-M. Rost, Phys. Rev. A **67**, 062704 (2003).
[31] E. P. Månsson, D. Guénot, C. L. Arnold, D. Kroon, S. Kasper, J. M. Dahlström, E. Lindroth, A. S. Kheifets, A. L'Huillier, S. L. Sorensen, and M. Gisselbrecht, Nat. Phys. **10**, 207 (2014).
[32] M. Y. Amusia, I. S. Lee, and V. A. Kilin, Phys. Rev. A **45**, 4576 (1992).
[33] F. Zhou, Y. Ma, and Y. Qu, Phys. Rev. A **93**, 060501 (2016).
[34] Y. Ma, Z. Liu, F. Zhou, and Y. Qu, Phys. Rev. A **98**, 043417 (2018).
[35] Y.-L. Ma, F.-Y. Zhou, Z.-Q. Liu, and Y.-Z. Qu, Chin. Phys. B **27**, 063201 (2018).
[36] Y. Ma, F. Zhou, L. Liu, and Y. Qu, Phys. Rev. A **96**, 042504 (2017).
[37] Z. Liu, Q. Liu, Y. Ma, F. Zhou, and Y. Qu, Phys. Rev. A **103**, 063102 (2021).
[38] J. A. Tanis, J.-Y. Chesnel, F. Frémont, D. Hennecart, X. Husson, A. Cassimi, J. P. Grandin, B. Skogvall, B. Sulik, J.-H. Bremer, and N. Stolterfoht, Phys. Rev. Lett. **83**, 1131 (1999).
[39] J. A. Tanis, J.-Y. Chesnel, F. Frémont, D. Hennecart, X. Husson, D. Lecler, A. Cassimi, J. P. Grandin, J. Rangama, B. Skogvall, B. Sulik, J.-H. Bremer, and N. Stolterfoht, Phys. Rev. A **62**, 032715 (2000).
[40] J. Fedyk, K. Gokhberg, and L. S. Cederbaum, Phys. Rev. A **103**, 022816 (2021).
[41] J. H. McGuire, Phys. Rev. Lett. **49**, 1153 (1982).
[42] Y.-K. Kim and M. E. Rudd, Phys. Rev. A **50**, 3954 (1994).
[43] M. Chen, K. Reed, D. McWilliams, D. Guo, L. Barlow, M. Lee, and V. Walker, At. Data Nucl. Data Tables **65**, 289 (1997).
[44] S. M. Younger, Phys. Rev. A **26**, 3177 (1982).
[45] M. S. Pindzola, D. C. Griffin, and J. H. Macek, Phys. Rev. A **51**, 2186 (1995).
[46] P. Defrance, J. J. Jureta, T. Kereselidze, J. Lecointre, and Z. S. Machavariani, J. Phys. B: At. Mol. Opt. Phys. **42**, 025202 (2009).
[47] M. R. Talukder, A. K. Haque, and M. A. Uddin, Eur. Phys. J. D **53**, 133 (2009).
[48] C. Bélenger, P. Defrance, E. Salzborn, V. P. Shevelko, H. Tawara, and D. B. Uskov, J. Phys. B: At. Mol. Opt. Phys. **30**, 2667 (1997).
[49] V. Fisher, Y. Ralchenko, A. Goldgirsh, D. Fisher, and Y. Maron, J. Phys. B: At. Mol. Opt. Phys. **28**, 3027 (1995).
[50] Y.-H. Zhu, Y. Ma, Y. Wu, and J. Wang, J. Quant. Spectrosc. Radiat. Transfer **272**, 107740 (2021).